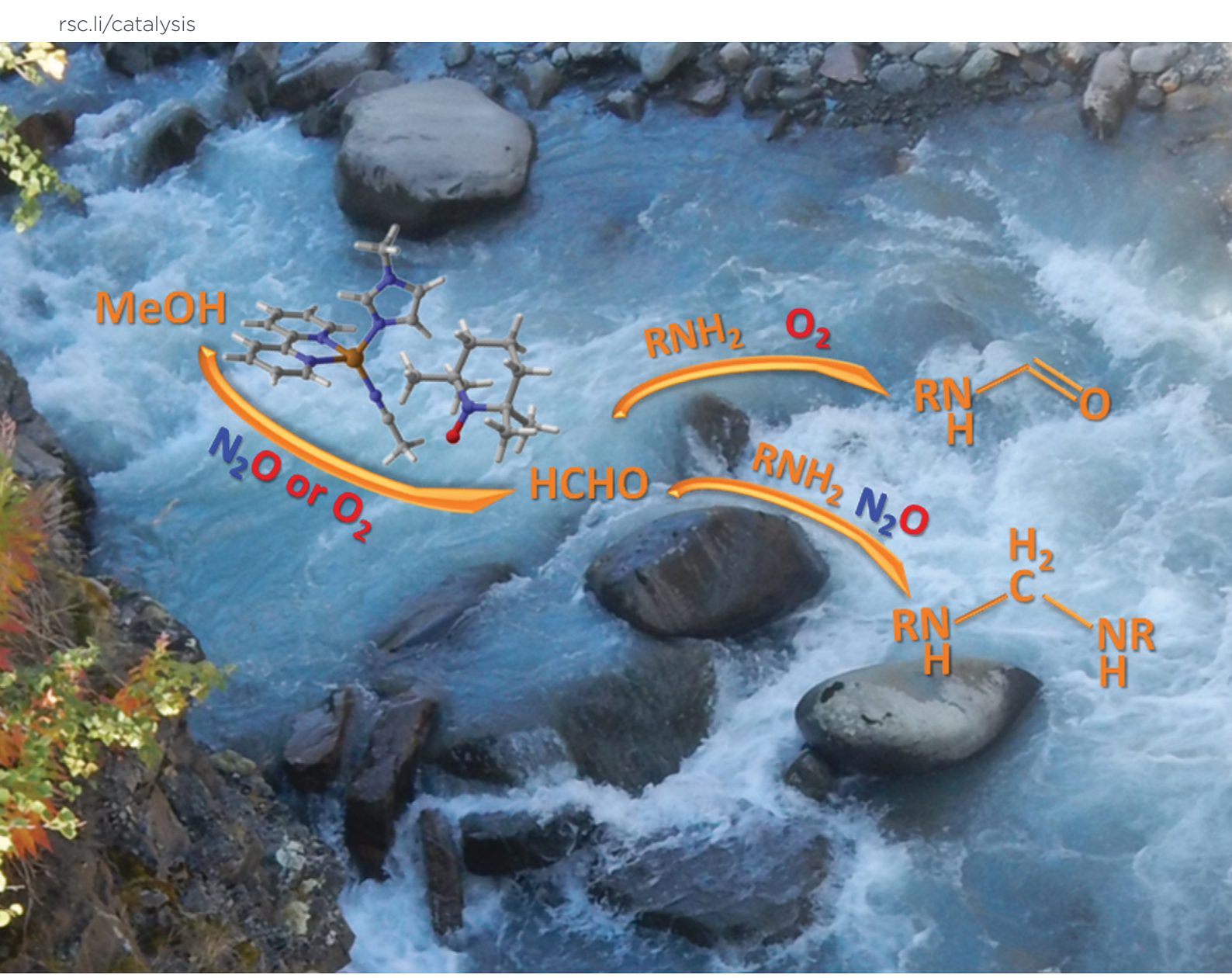
Volume 14 Number 22 21 November 2024 Pages 6433-6722

Catalysis Science & Technology



ISSN 2044-4761



PAPER

Catalysis Science & Technology



PAPER



Cite this: *Catal. Sci. Technol.*, 2024, **14**, 6503

Bioinspired copper-catalysed nitrous oxide reduction with simultaneous N-H or O-H bond oxidation†

Herein, we report on a bioinspired reduction of nitrous oxide in the presence of hydrogen-donating molecules, which are simultaneously oxidised. The copper-/TEMPO-based molecular catalyst has been previously reported to oxidise, for example, alcohols to aldehydes, diols to lactones, amines to imines, and, more recently, for the *N*-formylation of amines with methanol using (aerial) oxygen as a terminal oxidant. In this report, we demonstrate that it is possible to decompose nitrous oxide, a natural greenhouse gas and industrial waste gas, at low temperatures. This process simultaneously enables the oxidation of amines to imines and the formation of aminoacetal/aminal through the addition and oxidation of methanol. In this context, the Cu/TEMPO catalyst mimics nitrous oxide reductase (N2OR) and alcohol oxidase (AO) simultaneously. The catalyst is formed *in situ* from inexpensive and commercially available precursors. Selectivities and yields can be controlled by varying the composition of the substrate mixture and oxidant. This approach is attractive for the synthetic valorisation of organic molecules and utilisation of nitrous oxide, which remains a critical greenhouse gas and a byproduct of large-scale industrial processes, such as fertilizer production. These reactions, facilitated by a robust and affordable catalyst, are easy to carry out, making them highly practical for industrial applications.

Received 19th June 2024, Accepted 5th August 2024

DOI: 10.1039/d4cy00760c

rsc.li/catalysis

Introduction

Metal-catalysed biomimetic hydrogen evolution, oxidation and reduction reactions, ^{1–9} covering formaldehyde dehydrogenase (FADH), ^{1,2,8,9} formaldehyde dismutase (FDM)⁵ and deamination of nitriles, ⁷ have stimulated further exploration of biomimicries inspired by other related biological processes. Notably, aerobic processes often appear

† Electronic supplementary information (ESI) available: Experimental and instrumental details on synthesis, catalysis and characterisation, including NMR, MS, GC data and XYZ coordinate files of the DFT optimized molecular structures are available in the ESI. See DOI: https://doi.org/10.1039/d4cy00760c

more attractive than anaerobic ones owing to their robustness for practical application. For example, copper-containing enzymes can convert amines using oxygen as a terminal oxidant and hydrogen acceptor. Specifically, copper amine oxidases (CAOs)8,10,11 enable N-hydroxylation,12 whereas aldoxime dehydratases convert aldoximes to nitriles. 13-15 In this regard, in the past years, it has been well demonstrated that biomimetic catalysts inspired by copper oxidases with quinone co-factors or TEMPO (2,2,6,6-tetramethylpiperidine-N-oxyl radical) are able to activate amines and alcohols, giving access to aldehydes, lactones, imines and formamides with air or pure oxygen as terminal oxidant (Fig. 1).11,16-22 In a broader context, nitrogen-activating enzymes play a role in biological denitrification processes. Methane monooxygenase (MMO) and nitrous oxide reductase (N2OR) enable the decomposition of N₂O in the presence of CH₄. ^{23,24} N2OR also converts methanol to formaldehyde during denitrification while decomposing N₂O to N₂ and H₂O.²⁵ These MMO and N2OR enzymes often contain, for example, dicopper or diiron units.^{26,27} Studies on the catalytic cycle with a copper-based N2OR enzyme indicate that N2O coordinates to two Cu entities, and in the presence of proton sources under N2 evolution, a copper hydroxo species is formed during the cycle.²⁸ Copper hydroxo species are known to play a role in

^a Centro de Química Estrutural, Instituto Superior Técnico, Universidade de Lisboa, Av. Rovisco Pais 1, 1049-001, Lisboa, Portugal.

E-mail: martin.prechtl@tecnico.ulisboa.pt; Web: https://cqe.tecnico.ulisboa.pt; Web: https://www.h2.bio/

b Departamento de Química Fundamental, Instituto de Química, Universidade de São Paulo, Av. Prof. Lineu Prestes, 748 – Butantã, São Paulo, 05508-900, Brazil
 c Departamento de Engenharia Química, Instituto Superior de Engenharia de Lisboa, Instituto Politécnico de Lisboa, 1959-007 Lisboa, Portugal.
 E-mail: elisabete.alegria@isel.pt

^d Department of Synthesis and Analysis, Albert-Hofmann-Institute for Physiochemical Sustainability, Academy for the Advancement of Physiochemical Sustainability, Albert-Schweitzer-Str. 22, 32602 Vlotho, Germany. Web: https://www.a-h.institute

Selected related previous reports:

This work:

Fig. 1 Biological and biomimetic oxidation of C–O and C–N bonds. $^{1.27,11,16,17,19,21,22,25,34,35}$

alcohol and amine oxidation, which indicates the dual role of copper in coupled reduction and oxidation processes. 11 Moreover, it has been reported that $\rm N_2O$ is cytotoxic in vitamin B12-dependent metabolic cycles as it binds to and deactivates cobalamin, simultaneously leading to the degradation of $\rm N_2O$. 29,30 These observations are inspiring and significant for synthesis and energy conversion processes as $\rm N_2O$ is an abundant greenhouse and industrial waste gas. $^{23,31-33}$

The properties and lability of N_2O to decompose while acting as an H-acceptor in biological oxidation²⁵ motivated us to explore potential organometallic N2OR biomimetics.³⁴ In these studies, we demonstrated that the organometallic $\{[(p\text{-cymene})Ru](\mu\text{-H})(\mu\text{-Cl})(\mu\text{-HCO}_2)[Ru(p\text{-cymene})]\}BF_4$ complex, which is known to act as FADH and FDM mimic,^{1,2,5} exhibits activity as N2OR mimic with simultaneous oxidative dehydrogenation of amines to nitriles.³⁴ Consequently, we have been interested in determining if the Cu/TEMPO catalyst, previously used for

N-formylation¹¹ with methanol and oxygen as oxidants, can also reduce nitrous oxide and oxidise hydrogen-donating molecules containing NH and OH-bonds as co-factors, in particular alcohols and amines (Fig. 1).

Interestingly, in homogeneous catalysis, copper catalysts have not been extensively studied for N_2O reduction in oxidation reactions of alcohols or amines, and it is known that N2OR involves a Cu co-factor. 24,27,31,36,37 However, Yamada, 38 Severin, 39 Grützmacher 40 and their co-workers reported on the reduction of N_2O and oxidation of benzylic alcohols, 38,39 aliphatic alcohols 40 with Ru catalysts at elevated temperatures (100–150 °C) with moderate to good yields, 38,39 and high activity at lower temperatures (65–80 °C) for the oxidation of aliphatic alcohols. 40

In this study, we evaluated copper/TEMPO catalysts for the simultaneous reduction of N2O and the oxidation of amines and alcohols. These oxidative conversions, using nitrous oxide as a terminal oxidant, complement well our previous findings on the biomimetic oxidation of amines to nitriles with N₂O,³⁴ and the Cu/TEMPO-catalysed N-formylation with oxygen as an oxidant (Fig. 1).11 Interestingly, contrary to our expectations, we observed that N2O influences product selectivity in comparison to O2 as an oxidant in the case of methanol oxidation in the presence of amines, and the reagents do not undergo N-formylation, 11 but instead N,Naminoacetals (aminals) are formed selectively (Fig. 1). For the development of a simplified setup for amine oxidation, we disregarded the addition of gaseous ammonia to improve the selectivity, which is a typical workaround to shift the equilibrium in reduction and oxidation processes involving amines. 41,42 Instead, because we demonstrated previously that this is also possible by the application of polar protic solvents in (de)hydrogenation processes, we continue to further develop our previous protocols in this field to influence the selectivity in such processes with the solvent.4,7,41,43-45

Results and discussion

Synthesis of aminals, imines and aldehydes

In this work, we present a practical method to decompose N2O and synthesise imines and aminoacetals (aminals) using simple laboratory equipment and an easily accessible catalyst from commercially available precursors, [(bipy)Cu(NMI) (MeCN)]⁺I⁻ (bipy: bipyridine, NMI: *N*-methylimidazole, MeCN: acetonitrile), which is formed in situ in acetonitrile before the addition of TEMPO (2,2,6,6-tetramethylpiperidine-N-oxyl) as co-catalyst, substrates and oxidising agent. 11 Our previous studies on Cu/TEMPO catalysed N-formylation11 and the N2Oassisted studies on oxidation³⁴ helped us to estimate a starting point for the reaction conditions, reaction time and catalyst loadings. The N-formylation of benzylamine with methanol occurred with an 86% yield at 60 °C within 20 h with 5 mol% [Cu(bipy)NMI₂]⁺I⁻ (bipy: bipyridine, NMI N-methylimidazole) and 10 mol% TEMPO as catalyst precursors under an O₂ atmosphere.¹¹

Scheme 1 Optimised oxidation with N₂O of methanol in the presence of benzylamine. The formation of 4a with O_2 as an oxidant has been previously published by us. 11 *Spectroscopic yields for 2a, 3a and 4a with N₂O as oxidants were determined through ¹H NMR analysis with cyclohexane as an internal standard.

Because the active species are only present in low concentrations, we considered lower catalyst loading ([Cu]: 1 mol% and TEMPO: 2 mol%) as the starting point and short reaction times (2 h) to determine initial conversions of benzylamine (1.1 mmol) and methanol (2.2 mmol) under N₂O atmosphere at 60 °C. Interestingly, benzylamine 1a was fully converted in this reaction time, and the full aminal bis(benzylamino)methane 2a was formed as the major product, with a yield of 78%. In addition, N-benzylidenebenzylamine 3a (12%) and benzylformamide 4a (10%) were formed as side products (Scheme 1). The product distribution shows that methanol is oxidised to the formaldehyde level, and the majority readily reacts with the benzylamine to form the full aminal 2a; only a smaller

Table 1 Substrate scope for aminal formation

	2 h, -N ₂ , -H ₂ O	
Entry	Yield [%] aminal ^a	Yield [%] side product ^a
1	H H	3a (9%) 4a (7%)
2	2a, 84% (86%) ^b	4b (6%)
3	2b, 79% N N N H H H OMe MeO OMe	3c (25%)
4	2c,75%	3 d (6%)
5	2d, 79%	3e (11%)
6	2e, 54% (56%) ^b N N CF ₃	3f (12%)
7	2f, 64%	3g (13%)

[Cu] (1 mol%) TEMPO (10 mol%) N₂O, MeCN, 90°C, 2 h, -N₂, -H₂O

Reaction conditions: amine (1.1 mmol), MeOH (2.2 mmol), TEMPO (0.11 mmol) and 5 mL of the stock solution (equivalent to 1 mol% CuI, 2 mol% NMI, 1 mol% bipy), N₂O (100 mL condensed at -196 °C). All the reactions were performed in sealed 25 mL tubes. ^a Spectroscopic yields were determined by employing ¹H NMR analysis with cyclohexane as an internal standard. ^b Isolated yields after purification of 2a (column chromatography) and 2e and 2i (crystallisation).

2g, 84%

2h, 82%

2i, 75% (60%)^b

3h (18%)

3i (25%)

8

9

amount of the in situ-formed hemi-aminal is further oxidised to the corresponding N-formamide 4a. A decrease in the reaction temperature to 30 °C also gave similar results in terms of product distribution (2a:3a:4a = 77:10:13). Motivated by these results, we tentatively tried to shift the reaction by increasing the temperature to 90 °C with the target to improve the selectivity and maintain a short reaction time rather than a prolonged reaction time at lower temperatures. Under these conditions, the selectivity improved and bis(benzylamino)methane 2a was formed in 84% yield. In addition, N-benzylidenebenzylamine 3a (9%) and benzylformamide 4a (7%) were formed as side products, while no benzonitrile was formed in significant amounts (Scheme 1). Following the successful oxidation of methanol in the presence of amines with subsequent aminal formation, we considered the oxidation of benzylic alcohol 5a in the presence of amines with the same objective of aminal formation. However, no aminal was formed, benzaldehyde 6a was selectively formed instead. Similarly, in the absence of amines, benzaldehyde (yield: 99%) is the sole oxidation product of benzyl alcohol under similar mild conditions (40 °C for 2 hours under nitrous oxide) with mol% [Cu(bipy)NMI₂]⁺I⁻ (bipy: bipyridine, 5 N-methylimidazole) but only 5 mol% of TEMPO and no acetal is formed. More details on this aspect are summarised in Table 3 and in the related paragraph. Interestingly, with air as an oxidant, under similar conditions, the product selectivity was low and changed to a ratio of 45:15:0:35 (aminal:imine:formamide:nitrile). Therefore, under the optimised conditions for N2O, we tested a broader substrate scope (Table 1) of benzylamines with different functional groups and piperidine as cyclic aliphatic substrates. The reaction tolerates different substituents, including methoxy, alkyl and halide groups. Additionally, both electronwithdrawing and electron-donating groups are tolerated, as are varying degrees of substitution at the arene site. The yields and product selectivities vary from 54% to 84% for the aminal as the major product. The side products imine and formamide were detected with yields varying from 9% to 25% for imines for the benzylic amine substrates, and about 7% of formamides (4a-4b) and trace amounts of nitriles were qualitatively detectable by GC-MS (5d-5g).

Interestingly, regarding the aminal formation, isotopelabelled aminals with a CD₂-methylene entity are easily accessible through the use of labelled methanol, such as CD₃-OD (ESI,† section 2.4; D2-2a: D2-bis(benzylamino)methane 2a).

Notably, aromatic molecules with NH-entities, such as pyrroles, anilines or imidazoles, apparently do not undergo aminal formation, which indicates the selectivity for primary and secondary amines as substrates for this reaction. In addition, diamines, such as 1,2-cyclohexane diamine and pyrazine, were tentatively tested, but the corresponding bicyclic products were not determined. The precipitation of unidentified white solids may indicate the oligomerisation of such molecules under these conditions.

In addition to the oxidation of methanol in the presence of amines to aminals as major products, and the observation of the formation of imines as side products, we tested the oxidation of amines in the absence of methanol under similar conditions under an N2O atmosphere, yielding imines as products (Table 2). The tolerance of functional groups, steric hindrance and electronic properties of the substrates is similar to the observations for the aminal formation and N-formylation. 11 Thus, the major difference to other previously reported systems is only related to the previously oxidants. 11,17-19 Interestingly, reports homogeneously catalysed oxidation reactions with alcohols or amines as substrates, using nitrous oxide as the terminal oxidant and active transition metals such as ruthenium or rhodium, show different product selectivities. 31-34,38-40 For example, amines were oxidised to nitriles instead of imines,³⁴

Table 2 Substrate scope for imine formation

TEMPO (10 mol%)

Reaction conditions: amine (1.1 mmol), TEMPO (0.11 mmol) and 5 mL of the stock solution (equivalent to 1 mol% CuI, 2 mol% NMI, 1 mol% bipy), $\rm N_2O$ (100 mL condensed at –196 °C). All the reactions were performed in sealed 25 mL tubes. a Spectroscopic yields were determined using 1 H NMR analysis with cyclohexane as the internal standard.

3h, 43%

3i, 95%

and alcohols were converted to carboxylic acids or the corresponding esters. 32,33 In this regard, we were further encouraged to evaluate the present system for the oxidation of alcohols under nitrous oxide (Table 3).

Because benzaldehyde 6a was formed selectively from benzyl alcohol in the absence of amines (vide supra), we tested further benzylic alcohols under similar conditions (Table 3). Similar to aminal and imine formation, the reaction tolerates different substituents, including methoxy, alkyl and halide groups. Similarly, electron-withdrawing and electron-donating groups are tolerated, as are varying degrees of substitution at the arene site. Thus, the selectivity and efficiency are substrate-dependent and insignificantly dependent on the terminal oxidant. 16,17

Surprisingly, in contrast to our expectations from previous studies in polar protic solvent environments to shift the equilibrium in reduction and oxidation processes in the presence of water or OH-entities, 32,33,43,44,46,47 we did not observe the significant formation of carboxylic acids or esters through the addition of water. The major product formed continued to be the benzyl aldehyde as the major product. This underlines the product selectivity and robustness of the reaction but also limits the scope to tune the product selectivity through the solvent. Thus, further studies are required to enable the conversion of alcohols to carboxylic acids or esters in this manner.

Theoretic and mechanistic considerations

It is known that N2O can be activated through the coordination to the metal centre(s), where the N2O molecule could serve as a mono- or bidentate ligand. 48 The mechanistic data in this field is scarce. Moreover, the catalytic systems comprising both N2O and TEMPO are virtually unknown. Keeping in mind that the reduced form of TEMPOH is expected to participate in the catalytic cycle, we started our investigation with an inspection of possible reactions of N2O with TEMPOH. The GFN-FF force field 49 search for possible conformations of the {TEMPO + N2O} assembly through the CREST engine⁵⁰ resulted in a series of structures, from which the two lowest energy ones contained the N2O molecule for forming the O-H···O hydrogen bond with TEMPOH. The optimization of the first proposed structure using ORCA 5.0.4 software package⁵¹ (see the ESI† for further details) maintained the hydrogen bond but docked the N2O molecule closely to the TEMPOH one (intermediate 111-B, ESI†-Fig. S82). The overall free Gibbs energy for the formation of ¹I1-B relative to separate components is notably positive (7.0 kcal mol⁻¹). The search for the ¹⁻³MECP1-B configuration resulted in the angular geometry of the N₂O molecule with geometrical parameters close to those exhibited for the 1-3MECP1-A during unassisted N2O dissociation. The H-atom transfer to the oxygen atom of the N2O molecule proceeds without a transition state to form the ³I2-B intermediate featuring the

Table 3 Substrate scope for aldehyde formation

	Ph OH TEMPO (5 mol%) Ph OH TEMPO (5 mol%) Ph OH
	Ph OH N ₂ O, MeCN, 40°C, 5a-5I 2 h, -N ₂ , -H ₂ O 6a-6I
Entry	Yield [%] aldehyde ^a
1	0
2	6a, >99% MeO
	OMe
	6b, >82%
3	OMe
	6c ,99%
4	
	MeO ✓ ✓ 6d, >99%
5	
	(H ₃ C) ₂ HC 6e , >69%
6	0
	6f , >99%
7	
	6g, 94%
8	F
	F
9	6h, 73%
	¹Bu ¹
	6i , 64%
10	F ₃ C O
	CF ₃
11	6j , 78%
	Br
12	6k, 73%
	F
	6l , 88%

Reaction conditions: alcohol (1.1 mmol), TEMPO (0.055 mmol) and 5 mL of the stock solution (equivalent to 5 mol% CuI, 10 mol% NMI, 5 mol% bipy), N_2O (100 mL condensed at -196 °C). All the reactions were performed in sealed 25 mL tubes. a Spectroscopic yields were determined using ¹H NMR analysis with cyclohexane as an internal standard.

doublet-state HONN molecule coupled to a TEMPO radical (ESI†-Fig. S82). The HONN radical exhibited by intermediate 3 I2-B is unstable and undergoes decomposition to hydroxyl radical and molecular N_2 upon decoordination from TEMPO. It cannot be stabilized by making the hydrogen bond of the O–H group to water or acetonitrile molecules or another hydroxyl radical. Despite the overall negative ΔG of -7.0 kcal mol^{-1} , the activation energy ΔG^{\ddagger} between $\mathrm{^{1-3}MECP1-B}$ and $\mathrm{^{1}I1-B}$ of 43.1 kcal mol^{-1} (50.1 kcal mol^{-1} for $\mathrm{^{1-3}MECP1-B}$ and $\mathrm{^{1}R1-B}$ pair) indicates that copper-free activation of $\mathrm{N_2O}$ by TEMPOH is a rather unfavourable process.

Because the Cu-NNO compounds are known to be stable enough allow even their crystallographic characterization,⁵² we first modelled the respective complex bearing an opposite O-coordinated N2O molecule as an active intermediate. Attempts to optimize the putative singlet-state compound [(bipy)Cu(ONN)(NMI)]⁺ resulted in the expulsion of the N₂O molecule independently on the starting geometry or in the presence of additional ligands in the outer sphere (e.g. acetonitrile). However, the angular configuration of N2O that corresponds to the state with roughly equal energies of S_0 and T_1 states allowed for the stabilization of the [(bipy) Cu(ONN)(NMI)]+ molecule when considering it as an MECP structure. The free Gibbs energy gap ΔG^{\ddagger} between the intermediate ¹I1-C and ¹⁻³MECP1-C is 39.1 kcal mol⁻¹ (Fig. 2). Analysis of the spin density distribution of the triplet state of 1-3MECP1-C revealed its uniform distribution over the Cu-ONN fragment where the unpaired electrons are located on the $3d_{x^2-y^2}$ copper orbital and π^* molecular orbital of the coordinated ONN ligand. The optimization of the ¹⁻³MECP1-C geometry at the singlet surface affords the starting intermediate ¹I1-C, while the triplet surface optimization leads to the intermediate ³I2-C with very close geometry (Fig. 2) featuring slightly elongated O-N bond length ($\Delta d = 0.09 \text{ Å}$). Although the intermediate 3 I2-C shows a stable structure upon further optimization, the barrier 3 TS1-C between 3 I2-C and 3 I3-C (Fig. 2) has free energy very close to that of the starting 3 I2-C. This indicates that the lifetime of 3 I2-C under catalytic conditions should be quite short and that it undergoes N₂ elimination with the formation of the copper-oxyl product 1 P-C. The copper-oxyl species are known to be highly reactive and can abstract H atoms and activate hydrocarbons. 53 In the present case, product 1 P-C can easily oxidize TEMPOH without a notable barrier releasing the TEMPO radical. The respective transformation 3 I4-C \rightarrow 3 TS2-C \rightarrow 3 I5-C has an overall ΔG of 3 C6.7 kcal mol $^{-1}$ (ESI † -Fig. S83).

The addition of N2O ligand to the coordination sphere of copper in [(bipy)Cu(ONN)(NMI)]+ in an N-donor mode proceeds through the step of a supramolecular assembly (intermediate ¹I1-D, Fig. 3). The ¹⁻³MEPC1-D structure is located 33.3 kcal mol⁻¹ above the starting intermediate ¹I1-D, thereby showing lower ΔG^{\ddagger} values than those of pathway C (O-donor coordination). However, in contrast to pathway C, the reaction does not afford active intermediates that are isolated by the high reciprocal activation barrier. The geometry of intermediate ¹I1-D (Fig. 3) is quite close to that of ¹⁻³MEPC1-D. This is illustrated by the low difference in the single-point energies of the MECP and triplet intermediates (Fig. 3, inset). Therefore, while the ΔG^{\ddagger} activation for the N-donor coordination of the N₂O molecule (pathway **D**) is slightly lower than that for O-donor coordination (pathway C), the latter profile appears to be more favourable. It is worth noting that in contrast to the transition states, the energies of real spin-change transformations are lower due to spin-orbit coupling that makes spin-forbidden

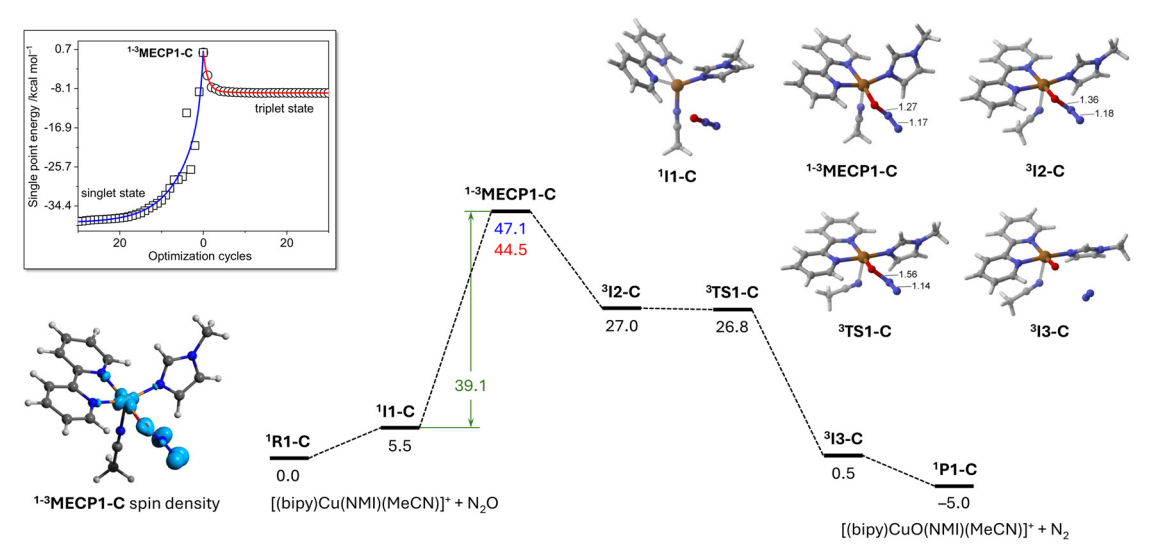


Fig. 2 Molecular structures, key interatomic distances (Å) and relative free Gibbs energies (kcal mol $^{-1}$) of the reaction profile between [(bipy) Cu(NMI)(MeCN)] $^{+}$ and N $_2$ O considering O-donor coordination mode. Blue (top) and red (bottom) energies for the MECP point designate those calculated at the singlet and triplet state for a given MECP geometry. The spin density isosurface is shown at the 0.02 a.u. level. The inset shows a decrease in the single-point energy upon optimization of the $^{1-3}$ MECP1-C structure at singlet or triplet surfaces.

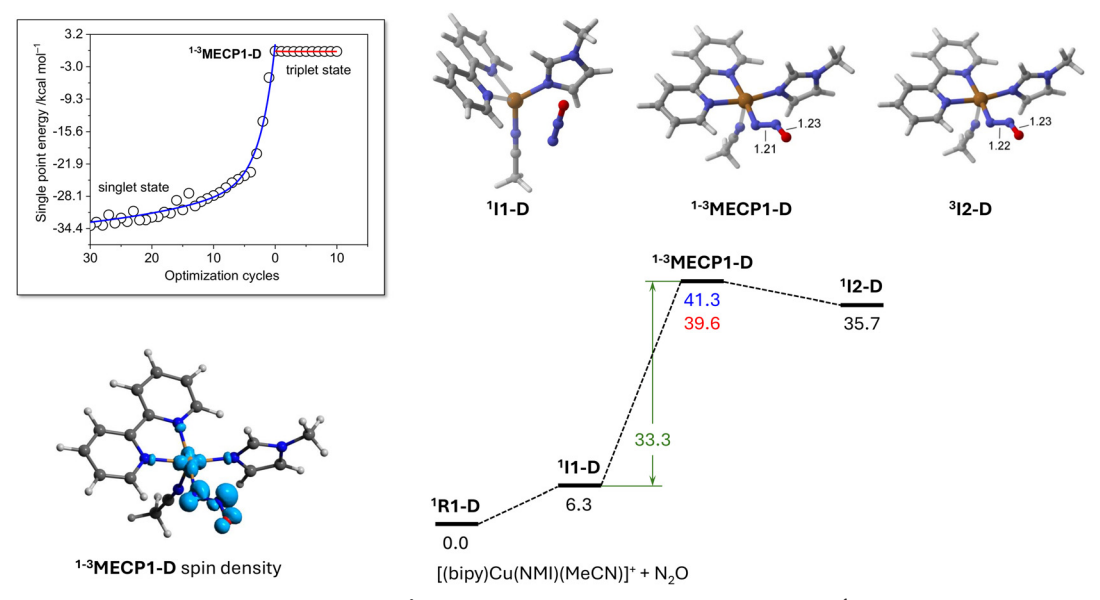


Fig. 3 Molecular structures, key interatomic distances (Å) and relative free Gibbs energies (kcal mol⁻¹) of the reaction profile between [(bipy) Cu(NMI)(MeCN)]⁺ and N₂O considering N-donor coordination mode. Blue (top) and red (bottom) energies for the MECP point designate those calculated at the singlet and triplet state for a given MECP geometry. The spin density isosurface is shown at the 0.02 a.u. level. The inset shows a decrease in the single-point energy upon optimization of the $^{1-3}$ MECP1-D structure at singlet or triplet surfaces.

transitions possible. 54,55 For example, for some metal coordination compounds, the difference between the expected MECP energies and true spin–orbit transition states can be more than 3 kcal mol^{-1} magnitude. 56 The barrier energies observed in the present case are similar to those found for $\mathrm{N_2O}$ activation, e.g. for the compounds of manganese. 57 One can conclude that the coordination of $\mathrm{N_2O}$ to a copper catalyst may produce active radicals that can oxidize alcohols and, in the framework of the present catalytic cycle, regenerate TEMPO radical from its reduced form.

Following the theoretical calculations and previous proposals for intermediates of Cu/TEMPO catalysed oxidation, 11,16-19,21,22,58 we tried to detect the newly proposed or related species (Fig. 2; i.e. [bipyCu(NMI)(N2O)(CH3O)]+, $[M]^+$ m/z = 376.07035) using high-resolution ESI-MS techniques. The HR-MS analyses (refer: ESI,† section 5, Fig. S67-S80) of aliquots taken from freshly prepared reactions in acetonitrile and catalyst stock-solution showed a range of signals that can be assigned to the intermediate (iminium ion, $[C_5H_{10}N=CH_2]^+$, $[M]^+$ m/z 98.0964), product (aminal, $(C_5H_{10}N)_2CH_2$, $[M-H]^+$ m/z 181.1699), and ligands (bipy, $C_{10}H_8N$; NMI, $C_4H_6N_2$). The iminium ion confirms the oxidation of methanol to formaldehyde. The latter readily reacts with amine to form the iminium ion, which is then converted into aminal by the reaction with another equivalent amine. In most cases, a range of signals with the isotope pattern of Cu⁶³/Cu⁶⁵ can be assigned to copper species carrying the bipy ligand and/or acetonitrile as a ligand. Interestingly, although the in situ formed species $[(bipy)Cu(NMI)(MeCN)]^+$ were identified in the past as having a central role in related Cu/TEMPO catalysed

oxidation reactions, the NMI as a labile ligand, acetonitrile as solvent and bipy as bidentate ligand apparently shifted the equilibrium, and the presence of [(bipy)₂Cu]⁺, [(bipy) Cu(MeCN)₂]⁺ and [Cu(MeCN)₄]⁺ can be confirmed by HR-MS (refer ESI†). Moreover, there are other copper species detectable by HR-MS, which can be assigned accordingly to species such as [bipyCuH]+ (C4H6N2CuH), [bipyCu(H2O)]+ or $[bipyCuH(OH)]^+$ $(C_4H_6N_2CuH_2O)$ and $[bipyCuN_2]^+$ $(C_4H_6N_2CuN_2)$. Considering the present catalytic oxidation conditions and previous studies, such species might play a role in the catalytic cycle. Another isotope pattern indicated a copper species tentatively assigned to [bipyCu(N₂O)H]⁺ (C₄H₆N₂CuN₂OH), which would be plausible with N2O as the oxidant, but the exact mass determined by HR-MS did not match exactly the theoretical mass and could not be confirmed. The same holds true for a proposed species with N₂O as ligand, [bipyCu(NMI)(N₂O)(CH₃O)]⁺ (Fig. 2, $[M]^{+}$ m/z = 376.0704). The observed signal at m/z 376.0693 with a typical isotope pattern for a copper species belongs to the parent [(bipy)2Cu]⁺ (ESI⁺-Fig. S71 and S80) and is detectable in the catalyst-stock solution in the absence of methanol and nitrous oxide (ESI†-Fig. S71). To rule out artefact signals, we also performed MS/MS fragmentation experiments, which showed that the isotope patterns assigned to the species [bipyCu(H₂O)]⁺ or [bipyCuH(OH)]⁺ (C₄H₆N₂CuH₂O) and [bipyCuN₂]⁺ stem from gas phase reactions induced under MS/MS conditions from the parent ion corresponding to [(bipy)₂Cu]⁺. Thus, although these species might play a role in the catalytic cycle, the MS/MS fragmentation experiments show that the presence of these species is related to the formation of those under ESI-MS conditions. Interestingly, the signals previously tentatively assigned to [bipyCu(N2O)H]+ did not appear in the MS/MS fragmentation experiments. Therefore, it is not apparently an

artefact, but its nature needs further clarification. In summary, the theoretical calculations and ESI-MS studies might be used as starting points for more detailed mechanistic studies, indicating the limitations of this system.

Conclusion and outlook

In summary, we assessed the oxidation of various benzylic amines and alcohols using nitrous oxide as an oxidation agent under mild conditions and compared our findings with the literature data. In the case of methanol oxidation with N₂O in the presence of amines, we observed the formation of aminals, contrasting N-formamides typically produced under O₂.¹¹ In addition, we demonstrated that N₂O can oxidise amines to imines and alcohols to aldehydes, showing similar product selectivities as Cu/TEMPO catalysts using oxygen or air as the terminal oxidant. A potentially interesting aspect is the simultaneous decomposition of the greenhouse gas nitrous oxide, which is a common by-product in the chemical industry. Thus, the Cu/TEMPO catalyst mimics N2OR and can decompose nitrous oxide in the presence of hydrogen donating molecules, such as alcohols and amines, producing aldehydes, imines or aminals, while nitrous oxide acts as a hydrogen acceptor and forms nitrogen and water. In addition, one needs to underline the dual role of the amines and methanol as protic substrates during methanol oxidation to stabilise the *in situ*-formed formaldehyde and trap it in the form of the aminal. In contrast, acetal formation does not seem to play a role in alcohol oxidation to aldehyde, and it would be interesting to convert methanol dialkoxymethanes under mild conditions with N2O because these compounds are of interest as combustion biofuel supplements.⁵⁹⁻⁶¹ The activation of nitrous oxide with such copper complexes is subject to further theoretical and experimental mechanistic studies to propose the reaction pathways for nitrous oxide decomposition and alcohol and amine oxidation. Another aspect of a more diverse synthetic application is based on the hydration of aldehydes because aldehydes in aqueous solvents are known to form geminal diols in high concentrations, which are readily converted into carboxylic acids under dehydrogenative or oxidative conditions. Further studies in this direction will open new possibilities for N2O decomposition with simultaneous carboxylic acid formation. ^{1,47} The authors anticipate that this work will widen the activities on N2O decomposition with bench stable molecular catalysts.

General experimental proceedings

The oxidation of benzyl amines and benzyl alcohols was tracked through ¹H nuclear magnetic resonance (NMR) analysis using a Bruker 400 MHz Avance II NMR spectrometer with a 5 mm BBO probe (d1 time = 1 s). Deuterated CDCl₃ was used as the solvent, and cyclohexane (20 µL, 0.184 mmol) served as the internal standard. For a comprehensive analysis, all reactions underwent GC-MS analysis using Clarus 600 (GC-MS) equipped with a Zebron

ZB-5 (Phenomenex) column measuring 30 m × 0.25 mm × 0.25 µm. The applied method involved a 14-minute temperature program: 2 minutes at 80 °C, followed by a ramp of 10 °C min⁻¹. to 120 °C, holding for 0 minutes, further ramping at 30 °C min⁻¹. to 300 °C, and then maintaining at 300 °C for 2 minutes. High-resolution mass spectrometry with electrospray ionization (HRMS-ESI) flow injection analyses (FIA) were performed by applying a Bruker Impact II quadrupole time-of-flight mass spectrometer equipped with an ESI† source (Bruker Daltoniks, Bremen, Germany), using sodium formate solution as an internal standard and acetonitrile as an eluent. All measurements were performed in the positive ion mode in the m/z 50–2000 range in the full scan or auto-MS/MS modes. The acquired data were processed using DataAnalysis 4.1 software (Bruker Daltoniks). Calibration was performed using a high-precision calibration mode (HPC). All theoretical masses and simulated spectra were calculated using Compass IsotopePattern (Bruker) or XCalibur FreeStyle (Thermo Scientific). The deuterated CDCl₃, benzylamines and benzyl alcohols were purchased from Tokyo Chemical Industry (TCI, Japan) and used without additional purification. The oxygen, nitrogen and nitrous oxide cylinders were obtained from Air Liquide. Silica (200 mesh) was used for column chromatography and monitored with TLC. For details on theoretical calculations and the software, refer to the ESI.†

Catalyst stock solution ([(bipy)Cu(NMI)(MeCN)]I)11

In a round bottom flask, CuI (0.212 mmol, 40.4 mg) was dissolved in 20 ml of acetonitrile. Afterwards, 2,2'-bipyridine (0.212 mmol, 33.1 mg) and NMI (0.44 mmol, 35.0 µL) were added. The reaction mixture was stirred for 30 minutes at room temperature, resulting in the formation of a dark green solution used directly for the oxidation reactions.

In some cases, the solution was also prepared at a lower concentration (see tables). 1 mL of stock solution was diluted in 4 mL of acetonitrile, yielding a solution with CuI (0.0424 mmol), 2,2'-bipyridine (0.0424 mmol) and NMI (0.088 mmol). The reaction mixture was stirred for 30 minutes at room temperature, resulting in the formation of a lighter green solution.

General procedure for aminal formation with N₂O

In a 25 mL tube equipped with a high-vacuum Teflon valve, TEMPO (16.7 mg, 0.11 mmol) was added along with 5 mL of the diluted stock solution (0.0424 mmol of CuI, 0.0424 mmol of 2,2'-bipyridine and 0.088 mmol of NMI). Following this, methanol (89 μL, 2.2 mmol or CD₃OD) and benzylamine (120 μL, 1.1 mmol) were introduced. The mixture was stirred under N2O. 100 mL of N2O was condensed into the tube at -196 °C. The flask was then heated to 90 °C for 2 hours (Scheme 1 and Table 1). After heating, the reaction mixture was allowed to cool to room temperature and was then carefully opened to release the solubilized gas. The reaction mixture was subsequently transferred to a round-bottom

flask, and acetonitrile was evaporated. Following evaporation, an internal standard of cyclohexane (20 µL, 0.184 mmol) and 50 μL of CDCl₃ were added to the solution. A portion (40 μL) of this mixture, along with 500 µL of CDCl₃, was then transferred to an NMR tube for ¹H NMR analysis.

General procedure for imine formation with N2O

In a 25 mL tube equipped with a high-vacuum Teflon valve, TEMPO (16.7 mg, 0.11 mmol or 8.4 mg, 0.055 mmol) was added along with 5 mL of the stock solution. Following this, benzylamine (120 µL, 1.1 mmol) was introduced. The mixture was stirred under N2O. 100 mL of N2O was condensed into the tube at -196 °C. The flask was then heated to the desired temperature (90 °C) for the specified duration (4 hours; Table 2). After heating, the reaction mixture was allowed to cool to room temperature and was then carefully opened to release the solubilized gas. The reaction mixture was subsequently transferred to a round-bottom flask, and acetonitrile was evaporated. Following evaporation, an internal standard of cyclohexane (20 µL, 0.184 mmol) and 50 μL of CDCl₃ were added to the solution. A portion (40 μL) of this mixture, along with 500 µL of CDCl3, was then transferred to an NMR tube for ¹H NMR analysis.

General procedure for aldehyde formation with N2O

In a 25 mL tube equipped with a high-vacuum Teflon valve, TEMPO (8.4 mg, 0.055 mmol) was added along with 5 mL of the stock solution (0.055 mmol of CuI, 0.055 mmol of 2,2'bipyridine and 0.11 mmol of NMI). Following this, benzyl alcohol (1.1 mmol) was introduced. The mixture was stirred under N2O. 100 mL of N2O was condensed into the tube at -196 °C. The flask was then heated to the desired temperature (40 °C) for the specified duration (2 hours). After heating, the reaction mixture was allowed to cool to room temperature and was then carefully opened to release the solubilized gas. The reaction mixture was subsequently transferred to a round-bottom flask, and acetonitrile was evaporated. Following evaporation, an internal standard of cyclohexane (20 µL, 0.184 mmol) and 50 µL of CDCl₃ were added to the solution. A portion (40 µL) of this mixture, along with 500 µL of CDCl₃, was then transferred to an NMR tube for ¹H NMR analysis.

Data availability

Experimental protocols and analytical/spectroscopic data are included as part of the ESI† of this article.

Author contributions

Synthesis and catalysis: BALS, SMPO, RSMA, MHGP; characterisation (experimental and simulation): BALS, SMPO, MHGP, DSN, AMMA; DFT theoretical characterisation: DSN; concept, funding acquisition, supervision, project administration: MHGP, ECBAA, LHA; writing - original draft: BALS, MHGP; writing - review & editing: BALS, MHGP; ECBAA.

Conflicts of interest

There are no conflicts to declare.

Acknowledgements

Authors thank FCT for the projects 2022.02069.PTDC (DOI: https://doi.org/10.54499/2022.02069.PTDC), UIDB/00100/2020 (DOI: https://doi.org/10.54499/UIDB/00100/2020), UIDP/00100/ 2020 (DOI: https://doi.org/10.54499/UIDP/00100/2020) and EXPL/QUI-QOR/1079/2021, (DOI: https://doi.org/10.54499/ EXPL/QUI-QOR/1079/2021) and contract IST-ID/086/2018 (D. S. N.) at the Centro de Química Estrutural, and LA/P/0056/ 2020 (DOI: https://doi.org/10.54499/LA/P/0056/2020) of Institute of Molecular Sciences, the Deutsche Forschungsgemeinschaft (DFG 411475421) the Centro de Química Estrutural/Institute of Molecular Sciences, Instituto de Química da Universidade de São Paulo (IQ-USP), Fundação de Amparo à Pesquisa do Estado de São Paulo (FAPES; 2019/10762-1), and Conselho Nacional de Desenvolvimento Científico e Tecnológico/Conselho Nacional de Pesquisas (CNPq, 312751/2018-4). The authors are grateful to Instituto Politécnico de Lisboa for the IPL/IDI&CA2023/ SMARTCAT_ISEL project.

Notes and references

- 1 L. E. Heim, N. E. Schloerer, J. H. Choi and M. H. G. Prechtl, Nat. Commun., 2014, 5, 3621, DOI: 10.1038/ncomms4621.
- 2 L. E. Heim, D. Thiel, C. Gedig, J. Deska and M. H. G. Prechtl, Angew. Chem., Int. Ed., 2015, 54, 10308-10312.
- 3 L. E. Heim, S. Vallazza, D. van der Waals and M. H. G. Prechtl, Green Chem., 2016, 18, 1469-1474.
- 4 D. van der Waals, L. E. Heim, C. Gedig, F. Herbrik, S. Vallazza and M. H. G. Prechtl, ChemSusChem, 2016, 9, 2343-2347.
- 5 D. van der Waals, L. E. Heim, S. Vallazza, C. Gedig, J. Deska and M. H. G. Prechtl, Chem. - Eur. J., 2016, 22, 11568-11573.
- 6 M. N. A. Fetzer, G. Tavakoli, A. Klein and M. H. G. Prechtl, ChemCatChem, 2021, 13, 1317-1325.
- 7 G. Tavakoli and M. H. G. Prechtl, Catal. Sci. Technol., 2019, 9, 6092-6101.
- 8 G. Tavakoli, J. E. Armstrong, J. M. Naapuri, J. Deska and M. H. G. Prechtl, Chem. - Eur. J., 2019, 25, 6474-6481.
- 9 M. Trincado, H. Grutzmacher and M. H. G. Prechtl, Phys. Sci. Rev., 2018, 3, psr-2017-0013.
- 10 D. M. Dooley, M. A. Mcguirl, D. E. Brown, P. N. Turowski, W. S. Mcintire and P. F. Knowles, Nature, 1991, 349, 262-264.
- 11 M. C. Pichardo, G. Tavakoli, J. E. Armstrong, T. Wilczek, B. E. Thomas and M. H. G. Prechtl, ChemSusChem, 2020, 13, 882-887.
- 12 H. Uehleke, *Xenobiotica*, 1971, 1, 327–338.
- 13 K.-I. Oinuma, Y. Hashimoto, K. Konishi, M. Goda, T. Noguchi, H. Higashibata and M. Kobayashi, J. Biol. Chem., 2003, 278, 29600-29608.
- 14 Y. Kato, S. Yoshida, S.-X. Xie and Y. Asano, J. Biosci. Bioeng., 2004, 97, 250-259.

- 15 S.-X. Xie, Y. Kato, H. Komeda, S. Yoshida and Y. Asano, Biochemistry, 2003, 42, 12056-12066.
- 16 J. M. Hoover and S. S. Stahl, J. Am. Chem. Soc., 2011, 133, 16901-16910.
- 17 B. L. Ryland and S. S. Stahl, Angew. Chem., Int. Ed., 2014, 53, 8824-8838
- 18 A. E. Wendlandt and S. S. Stahl, J. Am. Chem. Soc., 2014, 136, 506-512.
- 19 A. E. Wendlandt and S. S. Stahl, Org. Lett., 2012, 14, 2850-2853.
- 20 A. E. Wendlandt and S. S. Stahl, Angew. Chem., Int. Ed., 2015, 54, 14638-14658.
- 21 E. T. T. Kumpulainen and A. M. P. Koskinen, Chem. Eur. J., 2009, 15, 10901-10911.
- 22 Z. Hu and F. M. Kerton, Org. Biomol. Chem., 2012, 10, 1618-1624.
- 23 D. Mahor, Z. Q. Cong, M. J. Weissenborn, F. Hollmann and W. Y. Zhang, ChemSusChem, 2022, 15, e202101116.
- 24 S. R. Pauleta, M. S. P. Carepo and I. Moura, Coord. Chem. Rev., 2019, 387, 436-449.
- 25 K. Yamaguchi, A. Kawamura, H. Ogawa and S. Suzuki, J. Biochem., 2003, 134, 853-858.
- 26 M. O. Ross and A. C. Rosenzweig, J. Biol. Inorg. Chem., 2017, 22, 307-319.
- 27 T. Haltia, K. Brown, M. Tegoni, C. Cambillau, M. Saraste, K. Mattila and K. Djinovic-Carugo, Biochem. J., 2003, 369,
- 28 C. Carreira, S. R. Pauleta and I. Moura, J. Inorg. Biochem., 2017, 177, 423-434.
- 29 J. T. Drummond and R. G. Matthews, Biochemistry, 1994, 33, 3732-3741.
- 30 J. T. Drummond and R. G. Matthews, Biochemistry, 1994, 33, 3742-3750.
- 31 K. Severin, Chem. Soc. Rev., 2015, 44, 6375-6386.
- 32 T. L. Gianetti, S. P. Annen, G. Santiso-Quinones, M. Reiher, M. Driess and H. Grützmacher, Angew. Chem., Int. Ed., 2016, 55, 1854-1858.
- 33 P. Jurt, A. S. Abels, J. J. Gamboa-Carballo, I. Fernández, G. Le Corre, M. Aebli, M. G. Baker, F. Eiler, F. Müller, M. Wörle, R. Verel, S. Gauthier, M. Trincado, T. L. Gianetti and H. Grützmacher, Angew. Chem., Int. Ed., 2021, 60, 25372–25380.
- 34 B. A. L. Sacchelli, R. S. M. Almeida, A. G. Mahmoud, D. S. Nesterov, L. H. Andrade, A. M. M. Faisca Phillips, E. C. B. A. Alegria and M. H. G. Prechtl, Catal. Sci. Technol., 2024, 14, 1512-1523.
- 35 K. Yamaguchi, H. Ogawa, A. Kawamura and S. Suzuki, J. Inorg. Biochem., 2003, 96, 252-252.
- 36 W. Shen, H. Xue, N. Gao, Y. Shiratori, T. Kamiya, T. Fujiwara, K. Isobe and K. Senoo, Biol. Fertil. Soils, 2020, 56, 39-51.

- 37 J. L. Martinez, J. E. Schneider, S. W. Anferov and J. S. Anderson, ACS Catal., 2023, 13, 12673-12680.
- 38 K. Hashimoto, Y. Kitaichi, H. Tanaka, T. Ikeno and T. Yamada, Chem. Lett., 2001, 922-923.
- 39 A. G. Tskhovrebov, M. Solari, R. Scopelliti and K. Severin, Organometallics, 2012, 31, 7235-7240.
- 40 J. Bösken, R. E. Rodriguez-Lugo, S. Nappen, M. Trincado and H. Grützmacher, Chem. - Eur. J., 2023, 29, e202203632.
- 41 J. H. Choi and M. H. G. Prechtl, ChemCatChem, 2015, 7, 1023-1028.
- 42 M. Olivares, P. Knörr and M. Albrecht, Dalton Trans., 2020, 49, 1981-1991.
- 43 H. Konnerth and M. H. G. Prechtl, New J. Chem., 2017, 41, 9594-9597.
- 44 H. Konnerth and M. H. G. Prechtl, Green Chem., 2017, 19, 2762-2767.
- 45 M. H. G. Prechtl, J. D. Scholten and J. Dupont, J. Mol. Catal. A: Chem., 2009, 313, 74-78.
- 46 J.-H. Choi and M. H. G. Prechtl, ChemCatChem, 2015, 7, 1023-1028.
- 47 J. H. Choi, L. E. Heim, M. Ahrens and M. H. G. Prechtl, Dalton Trans., 2014, 43, 17248-17254.
- 48 W. B. Tolman, Angew. Chem., Int. Ed., 2010, 49, 1018-1024.
- 49 S. Spicher and S. Grimme, Angew. Chem., Int. Ed., 2020, 59, 15665-15673.
- 50 P. Pracht, F. Bohle and S. Grimme, Phys. Chem. Chem. Phys., 2020, 22, 7169-7192.
- 51 F. Neese, Wiley Interdiscip. Rev.: Comput. Mol. Sci., 2022, 12, e1606.
- 52 V. Zhuravlev and P. J. Malinowski, Angew. Chem., Int. Ed., 2018, 57, 11697-11700.
- 53 Y. Shimoyama and T. Kojima, Inorg. Chem., 2019, 58, 9517-9542.
- 54 J. W. Xu, J. Hao, C. J. Bu, Y. J. Meng, H. Xiao, M. Y. Zhang and C. S. Li, J. Chem. Theory Comput., 2024, 20, 3590-3600.
- 55 J. N. Harvey, Phys. Chem. Chem. Phys., 2007, 9, 331-343.
- 56 C. A. Gaggioli, L. Belpassi, F. Tarantelli, J. N. Harvey and P. Belanzoni, Chem. - Eur. J., 2018, 24, 5006-5015.
- 57 M. X. Jiang and C. G. Liu, J. Mol. Graphics Modell., 2017, 73, 8-17.
- 58 J. M. Hoover, B. L. Ryland and S. S. Stahl, ACS Catal., 2013, 3, 2599-2605.
- 59 K. Thenert, K. Beydoun, J. Wiesenthal, W. Leitner and J. Klankermayer, Angew. Chem., Int. Ed., 2016, 55, 12266-12269.
- 60 W. Ahmad, F. L. Chan, A. L. Chaffee, H. Wang, A. Hoadley and A. Tanksale, ACS Sustainable Chem. Eng., 2020, 8, 2081-2092.
- 61 R. Sun, I. Delidovich and R. Palkovits, ACS Catal., 2019, 9, 1298-1318.